10th World Congress on Structural and Multidisciplinary Optimization
May 19 - 24, 2013, Orlando, Florida, USA

Static Aeroelastic Stiffness Optimization and Investigation of Forward Swept Composite Wings

J.K.S. Dillinger[1], M.M. Abdalla[2], T. Klimmek[3], Z. Gürdal[4]

[1] DLR–Institute of Aeroelasticity, Göttingen, Germany, johannes.dillinger@dlr.de
[2] Delft University of Technology, Delft, The Netherlands, m.m.abdalla@tudelft.nl
[3] DLR–Institute of Aeroelasticity, Göttingen, Germany, thomas.klimmek@dlr.de
[4] University of South Carolina, Columbia, South Carolina, USA, gurdal@cec.sc.edu

1. Abstract
In this paper we present a detailed investigation of the aeroelastic optimization of swept forward composite wings. The wing is allowed to have variable stiffness, i.e., a varying thickness and stiffness matrices in the wing skins, and the use of balanced and unbalanced laminates is considered. Aside from common mass and stress responses, aeroelastic responses like aileron effectiveness, divergence and wing twist are also considered. Taking mass as an objective function, different sets of constraints on the structural and aeroelastic responses are investigated. The influence of minimum aileron effectiveness, divergence pressure and twist on the wing skin mass is analyzed. Load alleviation is a direct consequence of the mass objective and inherent to optimization with aeroelastic loads. Therefore is not necessary to consider it explicitly as a response. The essential difference of balanced and unbalanced laminates with their effects on mass and stiffness distribution is presented, and the influence of leading edge sweep angle on the optimized skin masses is investigated, subject again to variable sets of constraints.
2. Keywords: stiffness optimization; forward swept wing; aeroelastic tailoring; composite

3. Introduction

Forward swept wings with their beneficial influence on laminar flow, and therefore drag reduction and performance increase, have recently seen a resurgence in interest from the research community and industry. The unfavorable structural behavior of such wings resulting from the coupling of bending and torsion, however, aggravates the problem of designing a wing that can aerodynamically outperform classical designs. Yet, in conjunction with matured production technologies in the field of automated fiber placement and steering, new opportunities are arising to deal with these detrimental aeroelastic effects.

The optimization of composite materials applied in the load carrying structure of a wing is a research topic that has already been discussed for decades, see for example Starnes Jr et al. [1]. Aeroelastic effects in the optimization of wing structures has also been investigated to a large extent. An early overview on optimization technologies is provided in Vanderplaats et al. [2], while Shirk et al. [3] present a general overview on aeroelastic tailoring. Green [4] investigated the influence of nonsymmetric laminates on the aeroelastic behavior of high aspect ratio wings, while Ringertz [5] performed mass optimizations with a subsequent consideration of imperfections sensitivities. Eastep et al. [6] investigated the influence of layup orientation in a straight fiber design including aeroelastic constraints.

The first investigations into the selective application of composite material in forward swept wings for the purpose of divergence elimination were performed in the mid $1970's$ by Krone [7]. He showed that, by tailoring the properties of the material used in a wing, a considerably lower structural wing weight could be obtained compared to equivalent aluminum wings, even for large sweep angles. This work was extended by Weisshaar [8, 9], who has done detailed investigations into the effect of the spanwise stiffness distribution and bending-torsion coupling on divergence velocity, aileron effectiveness and spanwise center of pressure.

The laminate stiffness matrices resulting from classical lamination theory are traditionally expressed as a function of fiber angles and layer thicknesses. Another possibility exists to express the stiffness matrices as function of the lamination parameters, as described for example in Gürdal et al. [10]. The linear dependency of the stiffness matrices with respect to lamination parameters exhibits the advantage of a smoother design space in structural optimization problems. Their application in structural optimization problems has been investigated e.g. by Miki et al. [11] and Fukunaga et al. [12]. The boundaries within which the lamination parameters are allowed to vary to ensure feasible stiffness matrices is, for example, investigated by Setoodeh et al. [13]. Lamination parameter based optimization of plates for maximum

buckling load, minimum compliance, maximum fundamental frequency, and maximum strength is described in [14] – [20]. Herencia et al. [21] present an aeroelastic optimization without explicit aeroelastic constraints, for a wing box.

A stiffness optimization based on lamination parameters and including aeroelastic responses is given in Kameyama et al. [22] for a composite plate wing, while Thuwis et al. [23] investigated the passive drag reduction using a lamination parameter optimization applied on a Formula One wing. Minimizing the compliance of a variable-stiffness slender wing, modeled as a beam is demonstrated in Abdalla et al. [24].

In [25] the authors introduce an efficient method for composite stiffness optimization using aeroelastic constraints, along with commonly used sizing constraints like strain and buckling. The present paper constitutes a report on the application of this method to an aeroelasticity driven design of forward swept wings. An overview on the optimization methodology is given in Sec. 4, and the generation of the required finite element and optimization model, along with the derivation of response approximations as required by the optimization algorithm is described in Sec. 5. The influence of the three aeroelastic constraints aileron effectiveness, divergence and twist on optimized wing box mass is investigated, and a summary of the results is presented in Sec. 6.

4. Optimization Methodology

Various methods can be used to optimize composite structures, for this work we chose to separate the problem into three consecutive parts. The advantage of this strategy is that it allowed us to use the most suitable optimization tools for each of the different parts of the optimization process. The first part comprised an optimization based on stiffness matrices and laminate thicknesses. This part was treated in the present research and will be discussed in more detail below. The second part involved a stacking sequence optimization on the basis of the optimal stiffnesses derived in the first part. The third part dealt with the optimal conversion of stacking sequences to fiber paths suitable for the chosen production technology, e.g. fiber placement. Parts two and three do not depend significantly on the physics of the problem and are not discussed in this report. They are subjects of research at Delft University of Technology, see [26] – [29]; IJsselmuiden [30] provides a detailed overview of all three optimization steps.

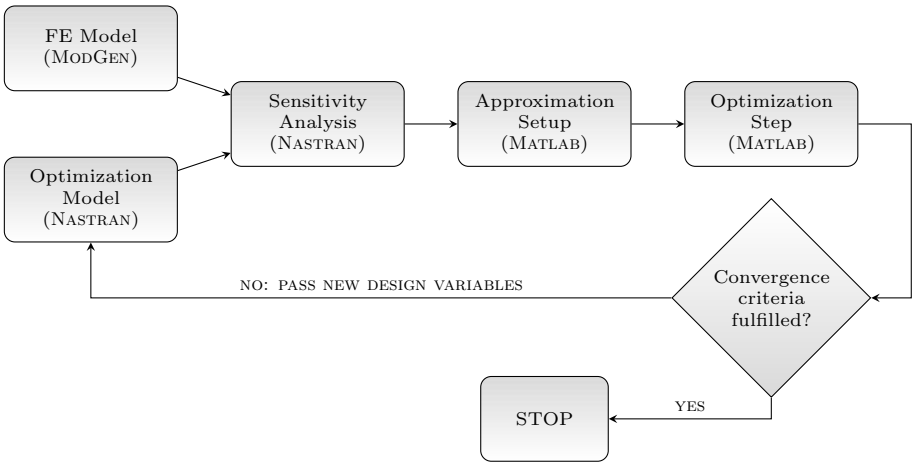

Figure 1: Stiffness optimization process

An overview of the disciplines involved in a stiffness optimization of the shell-like components of a wing, including aeroelastic constraints, is depicted in Figure 1. The basis is a finite element model of the wing structure that serves as an analysis model for the required responses and sensitivities. The shell properties are represented as normalized membrane $\hat{A}$ and bending stiffness matrices $\hat{D}$. Along with the laminate thicknesses h, they form the design variables $\mathbf{x}$ in the optimization process. An optimization model is defined, specifying design variables and responses f in the terminology of the applied finite element code NASTRAN. In order to reduce the amount of function evaluation in the form of a consecutive finite element analysis, the finite element model is replaced by an approximation model, in which the required responses are approximated as function of the design variables, Equation (1). Once the sensitivities $\frac{\partial f}{\partial \mathbf{x}}$ are derived using NASTRAN, they are converted to linear, Ψ_i, and reciprocal, Φ_i, sensitivities with respect to the stiffness matrices, where superscripts ^{m} and ^{b} denote sensitivities with respect to membrane and

bending stiffness, respectively; α_i is the sensitivity with respect to the thickness design variable.

$$\tilde{f} = \sum_{i=1}^{N} \left(\hat{\Psi}_i^{\ m}\big|_0 : \hat{A}_i + \hat{\Psi}_i^{\ b}\big|_0 : \hat{D}_i + \Phi_i^m\big|_0 : A_i^{-1} + \Phi_i^b\big|_0 : D_i^{-1} + \alpha_i\big|_0 h_i \right) + C_0 \tag{1}$$

These convex, separable and conservative approximations form the basis for the problem tailored gradient based stiffness optimizer, which minimizes the objective $f_0(\mathbf{x})$ in the approximate sub-problem, while the remaining responses $f_i(\mathbf{x})$ act as constraints, Equation (2). $n = 1 \dots i$ denotes the number of responses, and $m = 1 \dots j$ the number of design variables with a lower x_j^L and an upper limit x_j^U.

$$\begin{aligned} &\min\ f_0(\mathbf{x}) \\ &f_i(\mathbf{x}) \leq f_i|_{max} \\ &x_j^L \leq x_j \leq x_j^U \end{aligned} \tag{2}$$

Internally the optimizer transforms the stiffness matrices into independent lamination parameters and takes care of the feasible regions within which they can be varied to yield feasible stiffness matrices. Thus, the number of variables per stiffness matrix can be reduced from six to two for balanced and three for unbalanced laminates. According to Equation (3) the optimization is stopped when the change of the objective function f_0 in subsequent, feasible iterations (l) drops below a specified threshold δ_{stop}.

$$\left| \frac{f_0\big|_{(l+1)} - f_0\big|_{(l)}}{f_0\big|_{(l)}} \right| \leq \delta_{stop} \tag{3}$$

If the convergence criterion is not met, the design variables are updated according to the optimized approximate solution and a new iteration starts with the generation of new sensitivities.

5. Model Description

The wing geometry, the finite element and optimization model, and the required response approximations are briefly outlined here.

5.1. Wing Geometry

The wing dimensions were inspired by the research conducted in the DLR project *LamAiR* [31, 32] in which the aim was to develop an A320 like configuration, featuring a forward swept wing with increased laminar flow regimes for reduced skin friction drag, and rear mounted engines. The leading edge sweep required to obtain an equivalent pressure drag behavior for increasing *Mach* number is considerably lower for a forward than for a backward swept wing. The decrease in cross flow as a result of decreased sweep angle helps to postpone the transition from laminar to turbulent flow, therefore promoting a forward swept wing when aiming at increased aerodynamic performance. The wing geometry and the position of the load carrying wing box within the planform are depicted in Figure 2. The initial leading edge sweep angle is $\xi = -16.8°$. In order to investigate the influence of sweep angle on the optimized wing skin masses, two additional wings were modeled with sweep angles of $-10.0°$ and $-3.2°$, respectively. All other parameters like span, root and tip chord, and therefore wing area, box-position and aileron location remained unchanged, ensuring the comparableness between the designs. The dihedral was fixed to 4.0°.

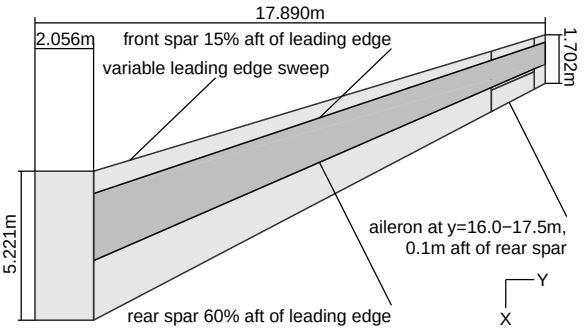

Figure 2: Planform (doublet lattice model) and wing box dimensions

5.2. Finite Element Model

The DLR–Institute of Aeroelasticity in-house tool ModGen [33] was used to generate the Nastran finite element (FE) models of the load carrying wing box. ModGen's parametric structure allows for a simple variation of e.g. the sweep angle by only a few changes in the standardized text input file.
The basis of the parametric process is formed by geometry models of the outer aerodynamic contour and

the structural entities defined within, like spars, ribs and stringers. Pursuant to the user defined input, the geometric entities are discretized with finite elements, comprising shell representations for skins, spars and ribs, and beam elements for the stringers.

Figure 3: FE model

The element properties required to complete the analysis model are included as well in the input file. Moreover, MODGEN generates the corresponding NASTRAN doublet lattice model for the computation of aeroelastic loads, along with a NASTRAN correction matrix to account for airfoil camber and geometric twist (*W2GJ* correction). Coupling of the aerodynamic and structural model is achieved using a load reference axis concept, consisting of a central node in each rib plane and two rigid elements extending from it to the leading and trailing edge. The central nodes are connected with interface elements to the boundary nodes of the rib they belong to. In addition to the three coupling nodes of the load reference axis, two additional points per rib on front and rear spar are selected. Accordingly, five structural nodes per rib plane exist, which are coupled to the aerodynamic model via NASTRAN `SPLINE1` cards.

Masses that are not part of the load carrying wing box were considered to be point masses, distributed in front and aft of the wing box along the span, and automatically attached via parameterized interfaces. To be able to construct meaningful optimization loadcases, it is essential to take a fuel model into consideration. MODGEN is able to determine the mass, inertia and center of gravity of all the rib-bay volumes, depending on user-defined filling levels and spanwise partitioning. Again, fuel could be modeled as point masses in their center of gravity and be attached to the structure with interface elements. A mass representing fuselage, tail, engines and payload was modeled in the symmetry plane and attached to the wing root. An overview on the finite element model as generated with MODGEN for a sweep angle of $\xi = -16.8°$ is provided in Figure 3. The applied airfoils exhibited a thickness variation from $\approx 14\%$ at the wing root to $\approx 11.5\%$ at the tip. Stringers extended in spanwise direction parallel to the front spar, and the pitch was set to 3% of the root chord, measured in chordwise direction. In total 25 ribs, including the ones at root and tip, were modeled and distributed equidistant in spanwise direction, aligned with the global x-axis. The element distribution in the wing skins was predetermined by the stringer and rib distance; each of these fields consisted of one shell element. This was required by the method used to derive the buckling factors and sensitivities.

Table 1: Laminate material properties

E_{11}	E_{22}	G_{12}	ν_{12}	ρ
$90.0e9\,GPa$	$7.05e9\,GPa$	$3.03e9\,GPa$	0.35	$1452\,kg/m^3$

All the structural components except for the stringers were modeled using the same carbon fiber material, the laminate properties of which are listed in Table 1. The initial thickness distribution of the wing skins was the same for upper and lower skin, comprising a linear variation from $25.0\,mm$ at the root to $5.0\,mm$ at the tip and a symmetric layup with $[-45_1/+45_1/90_2/0_6]_s$, where the angle subscripts denote the plies thickness contribution to the overall thickness. The ply angles were defined with respect to an axis that aligned with the average sweep of front and rear spar. The spar shear webs were modeled with a thickness variation from $20.0\,mm$ at the root to $15.0\,mm$ at the tip and a $[-45_7/+45_7/90_4/0_2]_s$ layup. The ribs had a constant thickness of $8.0\,mm$ and a quasi-isotropic symmetric layup $[\pm 45/90/0]_s$. According to classical lamination theory the stacking sequences were transformed to membrane and bending stiffness matrices, as requested by the optimizer. The stringers were modeled as beam elements made of titanium with a constant area of $6.08 * 10^{-4}\,m^2$ throughout the wing.

5.3. Optimization Model

In the context of this report, the term optimization model essentially denotes the setup of the required NASTRAN cards for the definition of the required design variables and responses, for which NASTRAN will compute sensitivities. The design variables consisted of six elements per membrane and bending stiffness

matrix, and the corresponding laminate thickness. In order to reduce calculation time, the elements were clustered to design fields, Figure 4, each of which comprised its own set of membrane and bending stiffness matrices, and a thickness. Upper and lower skin having the same design field resolution, the optimization model was made up of in total 70 design fields. The spars and ribs were not included in the optimization. With 13 design variables per design field, 910 design variables needed to be defined in NASTRAN. The computation of the strain and buckling factors and sensitivities for each element that is

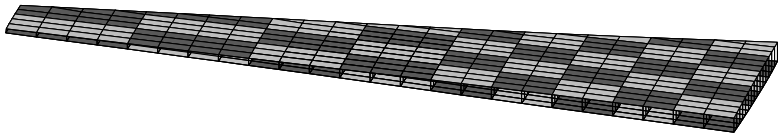

Figure 4: Design fields

part of the optimization model, necessitated the generation of stress responses in the two inplane and shear direction in their local element material coordinate systems. NASTRAN provides the responses at the lower and upper laminate end, eventually requiring six responses per element and loadcase. The FE model comprising 247 elements in each, upper and lower skin, led to 2964 NASTRAN stress responses per loadcase. Other NASTRAN responses included in the optimization were mass, aileron effectiveness as a combination of two aeroelastic stability derivatives, divergence and twist. The latter response was asked for at every node of the load reference axis; according to the amount of ribs at 25 spanwise locations.

5.4. Response Approximations

As mentioned in Sec. 4 and expressed in Equation (1), each response that would become either constraint or objective in the optimization was approximated as a linear and/or reciprocal function of the stiffness matrices and thickness. Physical insight into the response is required to select the most suitable contributions to its approximation. The optimizer demanding convex approximations, requires careful selection of the reciprocal contributions, which are not necessarily convex. A detailed overview of the approximation setup for strength, buckling, mass, aileron effectiveness and twist is provided in [25], therefore only a summary of the developed approximations, along with the wing specific divergence approximation, is given in Table 2.

Table 2: Response approximations

strength	$\tilde{r_i}$	$\simeq$	$\Phi_i^m : A_i^{-1} + \Psi_i^m : A_i + s_i^t \Delta N_i$
buckling	$\tilde{r_i}$	$\simeq$	$\Phi_i^b : D_i^{-1} + s_i^t \Delta N_i$
mass	$\tilde{m}$	$\simeq$	$\sum_j \alpha_j h_j$
aileron effectiveness	$\tilde{\eta}_{ail}$	$\simeq$	$\sum_j \Psi_j^m : A_j + \Psi_j^b : D_j + \Phi_j^m : A_j^{-1} + \Phi_j^b : D_j^{-1} + \alpha_j h_j$
twist	$\tilde{\vartheta}$	$\simeq$	$\sum_j \Psi_j^m : A_j + \Psi_j^b : D_j + \Phi_j^m : A_j^{-1} + \Phi_j^b : D_j^{-1} + \alpha_j h_j$
divergence	$\tilde{q}_{div}$	$\simeq$	$\sum_j \Psi_j^m : A_j + \Psi_j^b : D_j + \Phi_j^m : A_j^{-1} + \Phi_j^b : D_j^{-1} + \alpha_j h_j$

In the case of strength and buckling, the approximation of a failure index r_i was applied, based on a failure envelope criterion and a buckling theory for planar composite plates, respectively. Defining the strength failure envelope required that the maximum strain allowables were defined. Sensitivities $\Phi_i^m = \partial r_i / \partial A_i^{-1}$, $\Phi_i^b = \partial r_i / \partial D_i^{-1}$, $\Psi_i^m = \partial r_i / \partial A_i$ and $s_i^t = \partial r_i / \partial N_i$ were computed only based on the stress responses and sensitivities derived with NASTRAN. Load redistribution was accounted for in the change in force resultant, Equation (4). Failure indices are normalized quantities, with an upper limit at 1.0. If the index exceeds 1.0, the element will fail in the correspondent response.

$$\Delta N_i \simeq \sum_j \frac{\partial N_i}{\partial A_j} : A_j + \frac{\partial N_i}{\partial D_j} : D_j + \frac{\partial N_i}{\partial h_j} h_j \tag{4}$$

Mass only depends on thickness, and so does its approximation. In the absence of a direct relationship among the design variables and the aeroelastic responses, a sensitivity convexification was applied. For that purpose the reciprocal sensitivities $\Phi^m = -A\Psi^m A$ and $\Phi^b = -D\Psi^b D$ were checked for positive definiteness. If negative definite, the sensitivities were split up in a reciprocal and a linear sensitivity,

preserving as much of the reciprocal part as possible. The approximations of aeroelastic responses in Table 2 are therefore listed with all available sensitivity contributions.

6. Optimization Results

The results for a mass optimization of the load carrying wing box of forward swept wings subject to various sets of constraints are presented in this section. All optimizations applied the same set of loadcases, listed in Table 3. The four sizing loadcases $(1-4)$ corresponded to flight conditions on the admissible flight range boundary with variable altitude and load factor. The cruise loadcase (7) corresponded to the design *Mach* number and altitude. Aileron effectiveness, loadcases $(8-9)$, was calculated for velocities 15% above the admissible flight range velocities, and for the dive *Mach* number in case of velocities that would clearly violate the admissible range of the doublet lattice method, loadcase $(10-11)$. Finally, divergence pressure q_{div} was tested for the dive *Mach* number, loadcase (12).

Table 3: Load case definition

LC #	type	Ma [–]	q [Pa]	n_z [–]	H [m]
1	sym., push down, V_D	0.597	25300.0	-1.0	0
2	sym., pull up, V_D	0.597	25300.0	+2.5	0
3	sym., push down, M_D	0.870	22700.0	-1.0	6700
4	sym., pull up, M_D	0.870	22700.0	+2.5	6700
7	cruise, M_D	0.780	9700.0	+1.0	11900
8	antisym., roll, $1.15V_D$	0.690	33500.0		0
9	antisym., roll, $1.15V_D$	0.860	31900.0		4000
10	antisym., roll, V_D	0.870	22700.0		6700
11	antisym., roll, V_D	0.870	12000.0		11900
12	divergence, V_D	0.870			

In total, five different mass cases were considered, distinguished by two parameters fuel and passenger mass. Presumably the most unfavorable combination of empty wing tanks and maximum passenger load was considered for sizing loadcases $(1-4)$. The cruise loadcase (7) was investigated for a wing fuel loading approximately corresponding to begin/mid, and end of cruise flight, and for maximum and half passenger loading, totaling four more loadcases. The aileron effectiveness and divergence loadcase were independent of the mass distribution and could therefore be computed along with one of the depicted mass cases. The load and mass cases described above came down to one mass, 1976 strain failures, 3952 buckling failures, four twists, four aileron effectivenesses and one divergence response, summing to 5942 responses to be considered in the optimization. NASTRAN computed a far larger amount of responses, mainly due to the multiple stress responses required to calculate the failure indices. The sum of these responses was 12070. Along with the 910 design variables this led to $\approx 11\,Mio$ design sensitivities.

The wing with a nose sweep angle of $\xi = -16.8°$ will in the following be denoted the basic configuration, the wings comprising $\xi = -10.0°$ and $\xi = -3.2°$ nose sweep angle as configuration 1 and 2, respectively. The strain allowables required for the failure envelope construction were set to $[\varepsilon_t,\ \varepsilon_c,\ \gamma_{xy}] = [0.55\%,\ 0.70\%,\ 0.60\%]$. Along with the initial thickness distribution, described in Sec. 5.2, the strength and buckling failure indices could be computed for the sizing loadcases. The resulting failure indices had values considerably smaller than 1.0, which indicated that the starting design was well feasible and showed some potential for mass minimization.

Mass optimizations for all three wing configurations, always comprising the regular strength and buckling failure index constraints, along with one additional aeroelastic constraint will be presented in the following subsections. This approach allowed for an explicit distinction to be made of the influence of aeroelastic constraints on wing mass, and the effect of balanced and unbalanced laminates. In trying to converge to a global rather than a local optimum, two additional optimizations aside from the regular starting point were considered for each run, one comprising an altered thickness distribution and the other one a tilt of the initial laminate angles. The results shown in the following sections always take into consideration the run with the lowest mass of the three starting points. In most cases, the lowest mass was confirmed by at least one of the other starting points, also showing similar principal stiffness distributions in the majority of the design fields.

6.1. Aileron Effectiveness Constraint

Aileron effectiveness in this research was calculated as the negative ratio between roll coefficient due to aileron deflection and the roll coefficient due to rolling (roll damping), $\eta_{ail} = -C_{l_\delta}/C_{l_p}$, corresponding to

the tangent of the helix angle as described by the wing tip in a steady roll. According to this definition, aileron reversal occurs for $\eta_{ail} < 0$. Hence, the constraint was set as a lower limit, $\eta_{ail} \geq (\eta_{ail})_{min}$.

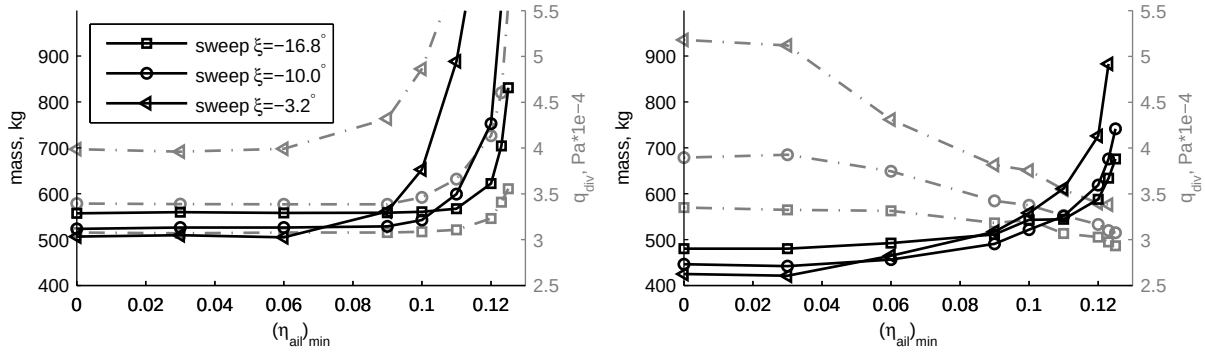

(a) balanced (b) unbalanced

Figure 5: Wing skin mass as function of aileron effectiveness $(\eta_{ail})_{min}$

The influence of aileron effectiveness constraints on the optimized wing skin mass is shown in Figure 5, separated into balanced and unbalanced laminate optimizations. Plotted in every point is the lowest of the four considered loadcases, compare Table 3. In addition, the plots show the appendant, unconstrained divergence pressure response. An important thing to notice is the weight benefit of unbalanced versus balanced laminates, amounting to $\approx 14 - 16\%$ at $(\eta_{ail})_{min} = 0$ for all sweep configurations. The weight gain for a decreased sweep angle was $\approx 9\%$, considering the basic configuration and configuration 2. For an increasing $(\eta_{ail})_{min}$ constraint the mass at first was not influenced, indicating that the constraint was not yet active. The basic configuration was influenced by $(\eta_{ail})_{min}$ only for higher constraint values. As a result, beyond a certain $(\eta_{ail})_{min}$ the conditions changed and the basic configuration featured the lowest mass. The unconstrained divergence pressure showed distinct differences between unbalanced and

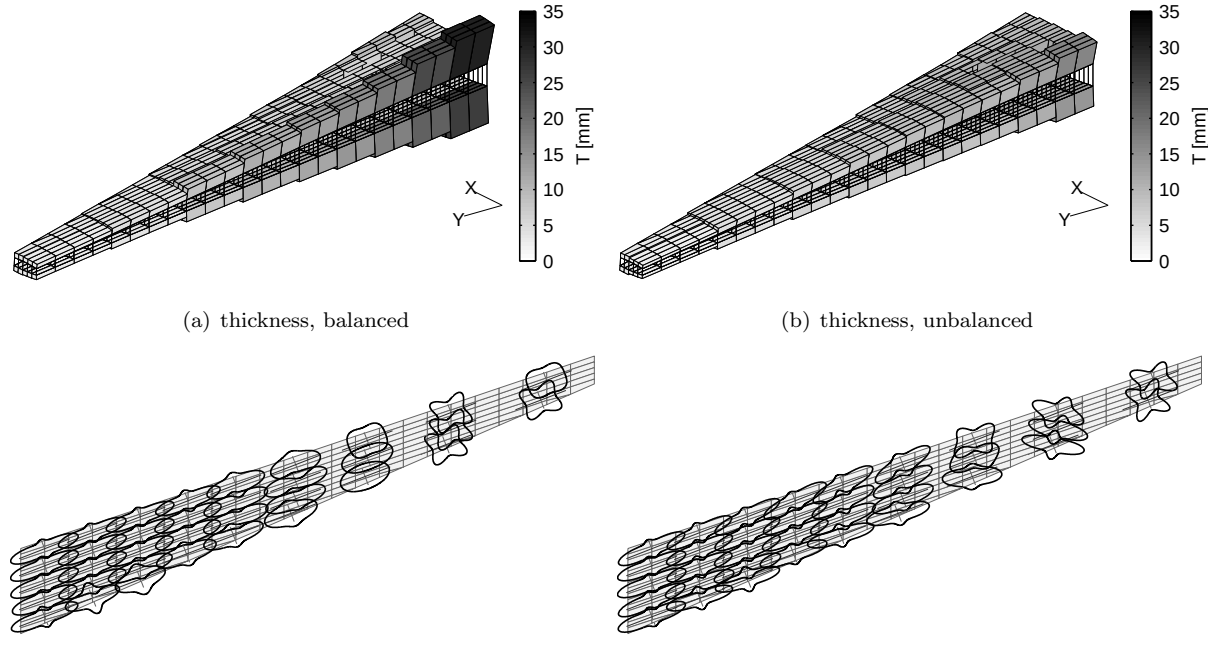

(a) thickness, balanced (b) thickness, unbalanced

(c) $E_{11}(\theta)$ top skin, balanced (d) $E_{11}(\theta)$ top skin, unbalanced

Figure 6: Basic Configuration, $(\eta_{ail})_{min} = 0.11$, optimized designs

balanced laminates. For unbalanced laminates the divergence pressure was considerably larger in case of configuration 2 and decreased quickly for increasing $(\eta_{ail})_{min}$ constraint. In case of balanced laminates the trend was the opposite, hence an increasing divergence pressure for increasing $(\eta_{ail})_{min}$ constraint.

The optimization results for a rather large $\eta_{ail} \geq 0.11$ are exemplified in Figure 6. To meet the constraint with balanced laminates, the thickness was increased in the frontal part, Figure 6(a), while in the case of unbalanced laminates the distribution was more consistent, Figure 6(b). Polar plots of the thickness normalized inplane engineering modulus of elasticity $\hat{E}_{11}(\theta) = 1/\hat{A}_{11}^{-1}(\theta)$, $\theta = 0$ to $360°$ of each laminate in the upper skin are depicted in Figures 6(c) and 6(d). Large extensions of the closed lines indicate an increased stiffness and therefore an increased amount of fibers in the corresponding direction. While for balanced laminates the distributions point out an increase in torsional stiffness in the outer wing, in the case of unbalanced laminates the constraint was met by tilting the main stiffness direction backwards, thereby introducing bending-torsion coupling.

6.2. Divergence Constraint

The influence of a divergence pressure constraint $q_{div} \geq (q_{div})_{min}$ on the optimized wing skin mass is summarized in Figure 7(a). In the case of balanced laminates, dashed lines, the influence of $(q_{div})_{min}$ is reflected in a weight increase with increasing divergence pressure. With increasing forward sweep the effect fortified. For unbalanced laminates, nearly no influence of the constraint on the wing skin mass could be noticed for the smaller forward sweep angles, configurations 1 and 2, suggesting that the constraint was nowhere active. While this is true for the smallest forward sweep angle $\xi = -3.2°$, it did become active for $\xi = -10.0°$ and $q_{div} \geq 40000\,Pa$, however, the optimization with unbalanced laminates was able to meet the constraint with nearly no weight increase.

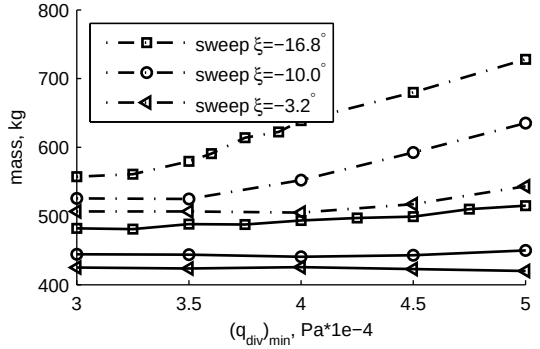

(a) Wing skin mass as function of divergence pressure q_{div}, balanced (dashed) and unbalanced (solid)

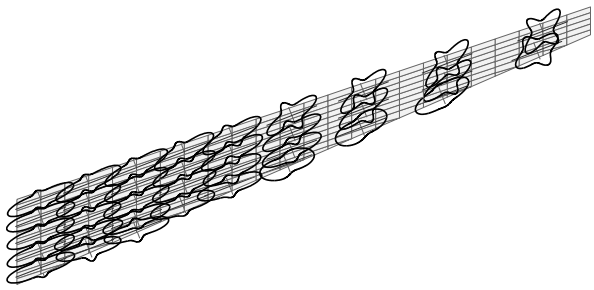

(b) Basic configuration, $E_{11}(\theta)$ top skin, unbalanced, $q_{div} \geq 40000\,Pa$

Figure 7: Divergence constraint

This is where unbalanced laminates can clearly outperform balanced laminates. The basic configuration with a forward sweep of $\xi = -16.8°$ exhibited $\approx 23\%$ weight saving for $q_{div} \geq 40000\,Pa$ when switching from balanced to unbalanced laminates and even more for larger divergence pressure constraints. The polar stiffness distributions for this case are plotted in Figure 7(b). Again, the optimizer introduced bending-torsion coupling, only this time in the opposite direction to that for the case of aileron effectiveness, Figure 6(d).

6.3. Twist Constraint

Contrary to divergence and aileron effectiveness, elastic wing twist is not constrained by aircraft regulations. Nevertheless, the wing twist distribution as function of span is an important aeroelastic parameter when it comes to optimal aerodynamic shape for minimum induced drag. Therefore, it was considered as a third aeroelastic constraint in the present investigation. With the tendency of a forward swept wing to increase aerodynamic twist when bending up, the twist constraint was set as an upper bound. Moreover, assuming the twist distribution to be of highest importance in cruise flight, for now only the tip twist in cruise was considered. Thus, the constraint can be written as $\alpha_{tip} \leq (\alpha_{tip})_{max}$. The results for balanced and unbalanced laminates are summarized in Figure 8. Again, a clear advantage in optimized mass existed for all three configurations with unbalanced laminates. While for $\alpha_{tip} \leq 1.0°$ a mass saving of $13 - 18\%$ could be achieved, the mass difference not only increased for smaller tip twist constraints, but with unbalanced laminates twist constraints could be reached that were unattainable with balanced laminates.

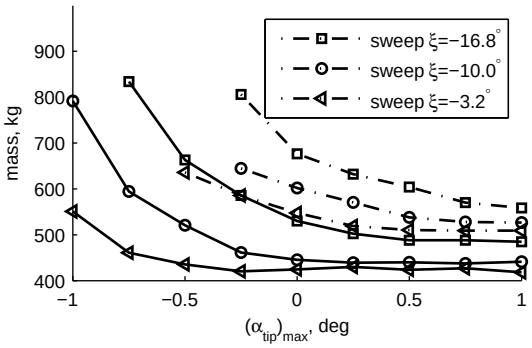

Figure 8: Wing skin mass as function of tip twist $(\alpha_{tip})_{max}$, balanced (dashed) and unbalanced (solid)

7. Summary

A detailed investigation into the influence of aeroelastic constraints and sweep angle on the optimized mass of three forward swept wings was presented. The wings featured equal wing area and span, and therefore also equal wing loading and aspect ratio. They were analyzed and optimized for a fixed set of mass and loadcases. The optimizer was shown to yield consistent results for balanced and unbalanced laminates. Unbalanced laminates showed clear advantages over balanced laminates for all aeroelastic constraints considered. The divergence constraint particularly, usually requiring a stiffened and therefore heavier wing structure in case of forward swept wings, was shown to incur no weight penalty when the structure is optimized using unbalanced laminates. It should be noted that results are expected to differ to some extent when spar webs are included in the optimization, or when varying the buckling field sizes/ratios. Eventually, the mass savings results presented in this report are supposed to show trends rather than absolute values of what is possible using unbalanced laminates. The source of largest possible errors remains to be the neglect of transonic effects in the application of a doublet lattice method. Inclusion of more accurate aerodynamic loads via incorporating an Euler solver in the design process is currently under investigation.

8. Acknowledgements

The optimization framework as described above is developed in the JTI Clean Sky SFWA project. Special thanks go to Yasser Meddaikar for his valuable contributions to model generation and optimization guidance.

9. References

[1] J. H. Starnes Jr and R. T. Haftka. Preliminary Design of Composite Wings for Buckling, Strength, and Displacement Constraints. *Journal of Aircraft*, 16(8):564–570, 1979.

[2] G. N. Vanderplaats and T. A. Weisshaar. Optimum design of composite structures. *International Journal for Numerical Methods in Engineering*, 27(2):437–448, 1989.

[3] M. H. Shirk, T. J. Hertz, and T. A. Weisshaar. Aeroelastic tailoring - Theory, practice, and promise. *Journal of Aircraft*, 23(1):6–18, 1986.

[4] J. A. Green. Aeroelastic tailoring of aft-swept high-aspect-ratio composite wings. *Journal of Aircraft*, 24(11):812–819, 1987.

[5] U. T. Ringertz. On structural optimization with aeroelasticity constraints. *Structural and Multidisciplinary Optimization*, 8(1):16–23, 1994.

[6] F. E. Eastep, V. A. Tischler, V. V.B., and N. S. Khot. Aeroelastic tailoring of composite structures. *Journal of Aircraft*, 36(6):1041–1047, 1999.

[7] N. J. J. Krone. Divergence Elimination with Advanced Composites. *AIAA paper*, 75-1009, 1975.

[8] T. A. Weisshaar. Divergence of Forward Swept Composite Wings. *Journal of Aircraft*, 17(6):442–448, 1980.

[9] T. A. Weisshaar. Aeroelastic Tailoring of Forward Swept Composite Wings. *Journal of Aircraft*, 18(8):669–676, 1981.

[10] Z. Gürdal, R. T. Haftka, and P. Hajela. *Design and optimization of laminated composite materials*. Of *A Wiley-Interscience publication*. Wiley, 1999.

[11] M. Miki and Y. Sugiyama. Optimum design of laminated composite plates using lamination parameters. *AIAA Journal*, 31(5):921–922, 1993.

[12] H. Fukunaga, H. Sekine, and M. Sato. Optimal Design of Symmetric Laminated Plates for Fundamental Frequency. *Journal of Sound and Vibration*, 171(2):219–229, 1994.

[13] S. Setoodeh, M. M. Abdalla, and Z. Gürdal. Approximate feasible regions for lamination parameters. In *Collection of Technical Papers - 11th AIAA/ISSMO Multidisciplinary Analysis and Optimization Conference*. Volume 2. Portsmouth, Virginia, 2006, pages 814–822.

[14] H. Fukunaga, H. Sekine, M. Sato, and A. Iino. Buckling design of symmetrically laminated plates using lamination parameters. *Computers and Structures*, 57(4):643–649, 1995.

[15] V. B. Hammer, M. P. Bendsoe, R. Lipton, and P. Pedersen. Parametrization in laminate design for optimal compliance. *International Journal of Solids and Structures*, 34(4):415–434, 1997.

[16] B. Liu, R. Haftka, and P. Trompette. Maximization of buckling loads of composite panels using flexural lamination parameters. *Structural and Multidisciplinary Optimization*, 26(1):28–36, 2004.

[17] S. Setoodeh, M. M. Abdalla, and Z. Gürdal. Design of variable-stiffness laminates using lamination parameters. *Composites Part B: Engineering*, 37(4-5):301–309, 2006.

[18] M. M. Abdalla, S. Setoodeh, and Z. Gürdal. Design of variable stiffness composite panels for maximum fundamental frequency using lamination parameters. *Composite Structures*, 81(2):283–291, 2007.

[19] S. T. IJsselmuiden, M. M. Abdalla, and Z. Gürdal. Optimization of Variable-Stiffness Panels for Maximum Buckling Load Using Lamination Parameters. *AIAA Journal*, 48(1):134–143, 2010.

[20] A. Khani, S. T. IJsselmuiden, M. M. Abdalla, and Z. Gürdal. Design of variable stiffness panels for maximum strength using lamination parameters. *Composites Part B: Engineering*, 42(3):546–552, 2011.

[21] J. E. Herencia, P. M. Weaver, and M. I. Friswell. Morphing Wing Design via Aeroelastic Tailoring. In *48th AIAA/ASME/ASCE/AHS/ASC Structures, Structural Dynamics, and Materials Conference*. (AIAA-2007-2217). Waikiki, Hawaii, 2007.

[22] M. Kameyama and H. Fukunaga. Optimum design of composite plate wings for aeroelastic characteristics using lamination parameters. *Computers and Structures*, 85(3-4):213–224, 2007.

[23] G. Thuwis, R. De Breuker, M. Abdalla, and Z. Gürdal. Aeroelastic tailoring using lamination parameters. *Structural and Multidisciplinary Optimization*, 41(4):637–646, 2010.

[24] M. M. Abdalla, R. De Breuker, and Z. Gürdal. Aeroelastic Tailoring of Variable-Stiffness Slender Wings for Minimum Compliance. In *IFASD 2007*. (IF-117). Stockholm, Sweden, 2007.

[25] J. K. S. Dillinger, M. M. Abdalla, T. Klimmek, and Z. Gürdal. Stiffness Optimization of Composite Wings with Aeroelastic Constraints. In *14th AIAA/ISSMO Multidisciplinary Analysis and Optimization Conference*. Indianapolis, Indiana, September 2012.

[26] S. T. IJsselmuiden, M. M. Abdalla, O. Seresta, and Z. Gürdal. Multi-step blended stacking sequence design of panel assemblies with buckling constraints. *Composites part b: engineering*, 40(4):329–336, 2009.

[27] J. Van Campen. Optimum lay-up design of variable stiffness composite structures. PhD Thesis. TU Delft, 2011.

[28] A. P. Nagy. Isogeometric design optimisation. PhD Thesis. TU Delft, 2011.

[29] J. M. J. F. van Campen, C. Kassapoglou, and Z. Gürdal. Generating realistic laminate fiber angle distributions for optimal variable stiffness laminates. *Composites part b-engineering*, 43(2):354–360, 2012.

[30] S. T. IJsselmuiden. Optimal Design of Variable Stiffness Composite Structures Using Lamination Parameters. PhD Thesis. TU Delft, 2011.

[31] A. Seitz, M. Kruse, T. Wunderlich, J. Bold, and L. Heinrich. The DLR Project LamAiR: Design of a NLF Forward Swept Wing for Short and Medium Range Transport Application. In *29th AIAA Applied Aerodynamics Conference*. Reston, Virigina, June 2011.

[32] M. Kruse, T. Wunderlich, and L. Heinrich. A Conceptual Study of a Transonic NLF Transport Aircraft with Forward Swept Wings. In *30th AIAA Applied Aerodynamics Conference*. New Orleans, Florida, June 2012.

[33] T. Klimmek. Parameterization of topology and geometry for the multidisciplinary optimization of wing structures. In *CEAS 2009 - European Air and Space Conference*. Manchester, UK, 2009.